Cell. Mol. Life Sci. (2017) 74:173–181
DOI 10.1007/s00018-016-2338-3

Cellular and Molecular Life Sciences

ORIGINAL ARTICLE

Ca^{2+} signals, cell membrane disintegration, and activation of TMEM16F during necroptosis

Jiraporn Ousingsawat[1] · Inês Cabrita[1] · Podchanart Wanitchakool[1] · Lalida Sirianant[1] · Stefan Krautwald[2] · Andreas Linkermann[2] · Rainer Schreiber[1] · Karl Kunzelmann[1]

Received: 17 February 2016 / Revised: 8 August 2016 / Accepted: 9 August 2016 / Published online: 17 August 2016

Abstract Activated receptor-interacting protein kinase 3 (RIPK3) and mixed lineage kinase domain like (MLKL) are essential components of the necroptotic pathway. Phosphorylated MLKL (pMLKL) is thought to induce membrane leakage, leading to cell swelling and disintegration of the cell membrane. However, the molecular identity of the necroptotic membrane pore remains unclear, and the role of pMLKL for membrane permeabilization is currently disputed. We observed earlier that the phospholipid scramblase and ion channel TMEM16F/anoctamin 6 cause large membrane currents, cell swelling, and cell death when activated by a strong increase in intracellular Ca^{2+}. We, therefore, asked whether TMEM16F is also central to necroptotic cell death and other cellular events during necroptosis. Necroptosis was induced by TNFα, smac mimetic, and Z-VAD (TSZ) in NIH3T3 fibroblasts and the four additional cell lines HT_{29}, 16HBE, H441, and L929. Time-dependent changes in intracellular Ca^{2+}, cell morphology, and membrane currents were recorded. TSZ induced a small and only transient oscillatory rise in intracellular Ca^{2+}, which was paralleled by the activation of outwardly rectifying Cl^- currents, which were typical for TMEM16F/ANO6. Ca^{2+} oscillations were due to Ca^{2+} release from endoplasmic reticulum, and were independent of extracellular Ca^{2+}. The initial TSZ-induced cell swelling was followed by cell shrinkage. Using typical channel blockers and siRNA-knockdown, the Cl^- currents were shown to be due to the activation of ANO6. However, the knockdown of ANO6 or inhibitors of ANO6 did not inhibit necroptotic cell death. The present data demonstrate the activation of ANO6 during necroptosis, which, however, is not essential for cell death.

Keywords Cell death · Necroptosis · Apoptosis · TMEM16F · Anoctamin 6 · Chloride channel

Electronic supplementary material The online version of this article (doi:10.1007/s00018-016-2338-3) contains supplementary material, which is available to authorized users.

✉ Karl Kunzelmann
karl.kunzelmann@ur.de

1 Institut für Physiologie, Universität Regensburg, Universitätsstraße 31, 93053 Regensburg, Germany

2 Division of Nephrology and Hypertension, Christian-Albrechts-University, Kiel, Germany

Introduction

Activation of ion channels is an essential step during regulated cell death [1]. Ion channels participate in execution of apoptosis and have also been assumed to be critical for necroptosis and other forms of caspase-independent cell death. Ion channels may shrink cells, thereby moving them towards apoptosis [2]. To induce apoptotic cell shrinkage, K^+ and Cl^- ions or osmotically active organic molecules are released from the cell [2]. Numerous K^+ channels are known to contribute to this process, and recent studies demonstrate the molecular identity of the underlying anion permeable channels as members of the LRRC8 family of proteins [3–5].

In contrast to apoptotic cell shrinkage, necroptosis is characterized by cell swelling and disintegration of the cell membrane [1, 6]. Membrane permeabilization is thought to be caused by nonselective ion channels that allow influx of NaCl and water leading to cell swelling. Apart from other theories, a plasma membrane-localized MLKL complex has been proposed to act as a cation influx channel or, alternatively, to activate other proteins to increase Na^+ influx and osmotic pressure, and to induce membrane rupture [7]. Because this concept is controversial [1], and knowledge about Ca^{2+} signaling and membrane currents in necroptosis is limited, we decided to analyze these parameters in more detail.

TMEM16F/anoctamin 6/ANO6 is a membrane-localized phospholipid scramblase and ion channel that has been implicated in apoptotic cell death induced by a large and steady rise in intracellular Ca^{2+} [8]. Activation of ANO6 was shown to generate membrane Cl^- currents that can induce apoptotic cell shrinkage (AVD; apoptotic volume decrease). However, cell swelling and cellular disintegration are observed upon pronounced increase in intracellular Ca^{2+}, which causes non-selectivity of ANO6 currents [8–10]. As the molecular nature of the necroptotic membrane channel remains obscure, we asked whether membrane permeabilization is due to the activation of ANO6. Although ANO6-typical membrane currents were activated during necroptosis, our present data indicate that the activation of ANO6 is not crucial for necroptotic cell death.

Results

Necroptosis was induced in NIH3T3 cells using TNFα, smac mimetic birinapant, and the pan-caspase inhibitor Z-VAD (TSZ) [11] (Fig. 1a, b). About 90 % of the cells were necroptotic after 4-h treatment with TSZ. Necroptotic cell death was completely inhibited by simultaneous treatment with necrostatin-1 (Nec-1) (Fig. 1b, c). Moreover, cell death was also induced by TSZ in L929 (murine skin fibroblasts), HT_{29} (human colonic epithelial cells), 16HBE (human bronchial epithelial cells), and H441 (human airway club cells) (Supplementary Fig. 1). Necroptosis was completely suppressed by 100 µM Necrostatin-1 (Nec-1) in all cell lines. In human epithelial cells, necroptotic cell death was also partially suppressed by 5 µM necrosulfonamide (NSA).

It is commonly accepted that cells swell during necroptosis, due to influx of NaCl and water. This ultimately leads to membrane disintegration and cell death [6]. As proper cell volume measurements are still missing, we decided to analyze cell volume and cell morphology using quantitative phase microscopy (QPM). QPM is using interference holographic images of unstained cells allowing for accurate and seamless assessment of the cell volume with very little time delay [12–14]. 3D images taken over four hours of TSZ treatment indicate that cells initially swell within the first hour, but then start to shrink (Fig. 2a, b). Cell shrinkage was inhibited by Nec-1 (Fig. 2b). Morphological and volume changes were also assessed using differential interference contrast (DIC) (Fig. 2c). The cell volumes were determined from individual cells using DIC images and cell height determined from bottom/top focal planes, using the software Axiovision (Zeiss, Munich). These data also indicate an initial cell swelling within the first hour of TZS application and subsequent cell shrinkage (Fig. 2d). To further confirm these volume changes, we used flow cytometry. 30,000 cells were exposed to TSZ (or kept in control solution) and analyzed in a CASY flow cytometer. The assays were repeated 3–9 times. The data again indicate an initial swelling within the first 2 h which then changes into cell shrinkage (Fig. 2e). Finally, we used online membrane capacitance measurements in patch clamp experiments as a fourth independent technique. The capacitances were recorded continuously and read directly from the instrument. Surprisingly, we found a large and significant increase in cell membrane capacitance, which is known to correlate to an increase in plasma membrane surface area (Fig. 2f). These results suggest that changes in cell morphology occur mainly due to unfolding of membrane invaginations [15] or membrane exocytosis, which may contribute to membrane disintegration. The data do not support the concept of a persistent cell swelling and do not suggest activation of large nonselective ion currents that would otherwise lead to massive cell swelling [16].

Cell volume was also measured in HT_{29} cells using quantitative phase microscopy and flow cytometry. HT_{29} epithelial cells are less susceptible towards necroptotic stimulation and were exposed to TSZ for 16 h to induce necroptosis (Supplementary Fig. 1). The data indicate that also HT_{29} cells swell within the first 4–5 h of TSZ exposure, but then start to shrink (Supplementary Fig. 2). Similar to NIH3T3 cells, the membrane capacitance is enhanced from 22.9 ± 3.1 to 34.8 ± 3.9 pF ($n = 9$). Similar swelling and subsequent shrinkage were observed for other cell lines (data not shown). Cell shrinkage was observed at later stages of necroptosis, i.e., several hours after exposure to TSZ. Cell shrinkage is actually a hallmark of apoptotic cell death [17]. To rule out a role of apoptosis, we induced necroptosis in the three different cell lines, NIH3T3 (mouse embryonic fibroblasts), L929 (murine skin fibroblast), and HT_{29} (human colonic carcinoma epithelial) cells using 100 ng/ml TNFalpha + 25 µM Z-VAD and 100 ng/ml TNF alpha + 25 µM + 1 µM Smac mimetics, respectively, and examined possible activation of apoptosis by Western blotting of Caspase-3. As a positive control, Jurkat T-lymphocytes were treated with 100 ng/ml alpha-Fas (clone 7C11; Immunotech) to induce apoptosis. Capase-3 Westerns demonstrated apoptosis in Jurkat cells, but complete absence of cleaved caspase-3 in necroptotic NIH3T3, L929, and HT_{29} cells. Apoptosis (cleaved caspase-3) in Jurkat cells was completely blocked by 25 µM Z-VAD (Supplementary Fig. 3). These data suggest that TSZ treatment indeed induced necroptosis.

Activation of Ca^{2+} permeable membrane channels and Ca^{2+} influx has been proposed as crucial events in necroptosis, and it has been suggested that Ca^{2+} influx

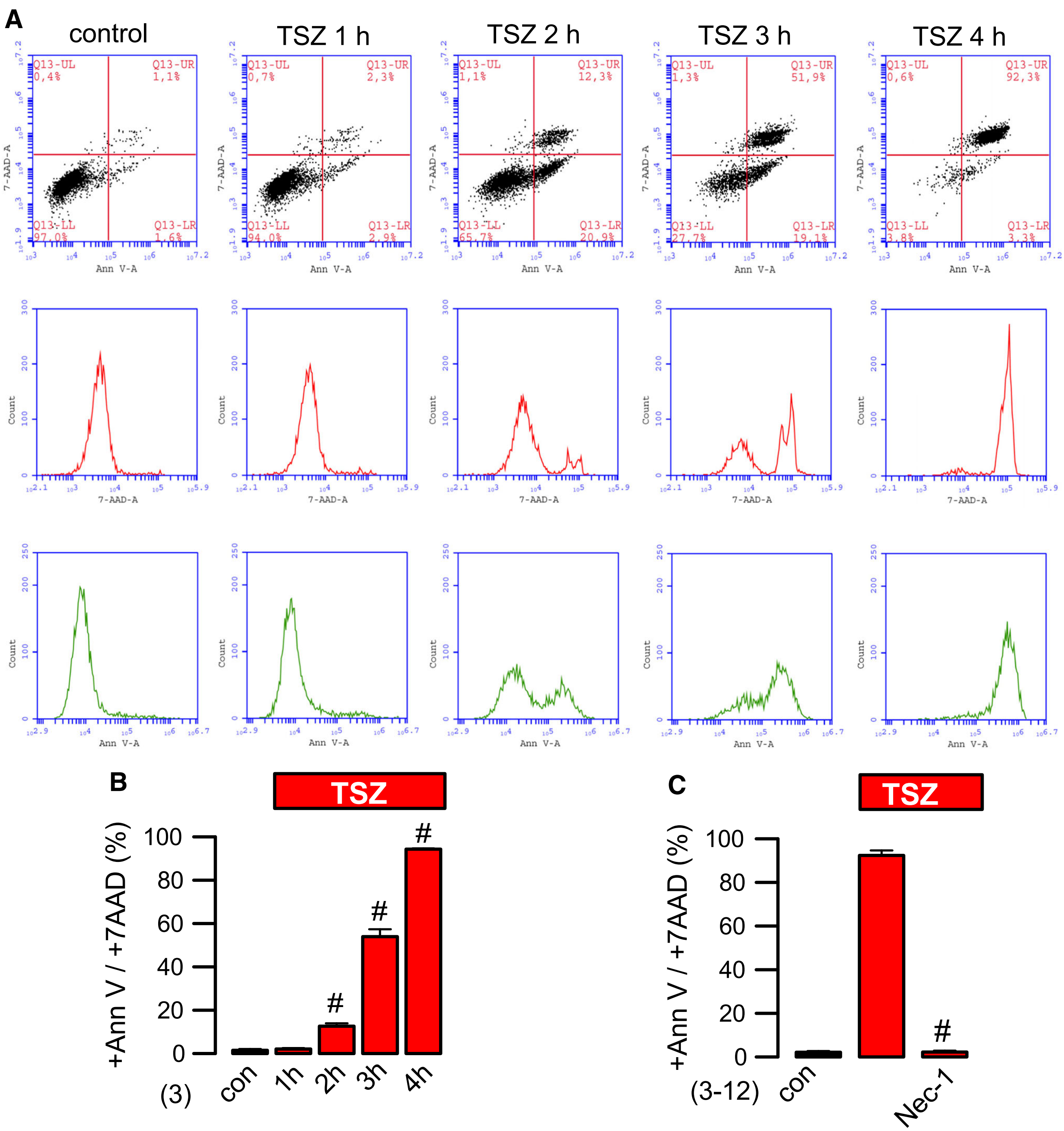

Fig. 1 Induction of necroptosis in NIH3T3 cells. Necroptosis in NIH3T3 cells was induced by the necroptotic cocktail TSZ containing TNF (10 ng/ml), smac mimetic birinapant (5 µM), and the pan-caspase inhibitor Z-VAD (25 µM). **a**, **b** Flow cytometry indicating time-dependent membrane permeabilization (7-AAD positivity) and phosphatidylserine exposure (annexin V positivity). **c** Inhibition of necroptosis (AnnV/7-AAD positivity) by necrostatin 1 (Nec-1; 100 µM). Mean ± SEM (number of cells). [#]Significant increase in AnnV/7-AAD positivity ($p = 0.002$, 2 h; 0.004, 3 h; 0.00001, 4 h) and inhibition by Nec-1 ($p = 0.00001$) (ANOVA)

occurs through TRPM7 channels [16]. We analyzed changes in intracellular Ca^{2+} occurring upon induction of necroptosis and found an only small increase in basal Ca^{2+} levels along with induction of Ca^{2+} oscillations (Fig. 3a, b). Increase in basal Ca^{2+} and Ca^{2+} oscillations was completely suppressed by dantrolene, an inhibitor of ryanodine Ca^{2+} release channels expressed in the endoplasmic reticulum (ER) membrane, while inhibitors of IP3 receptor/Ca^{2+} release channels (xestospongin C), TRPC membrane Ca^{2+} influx channels (SK&F96365), or TRPM7

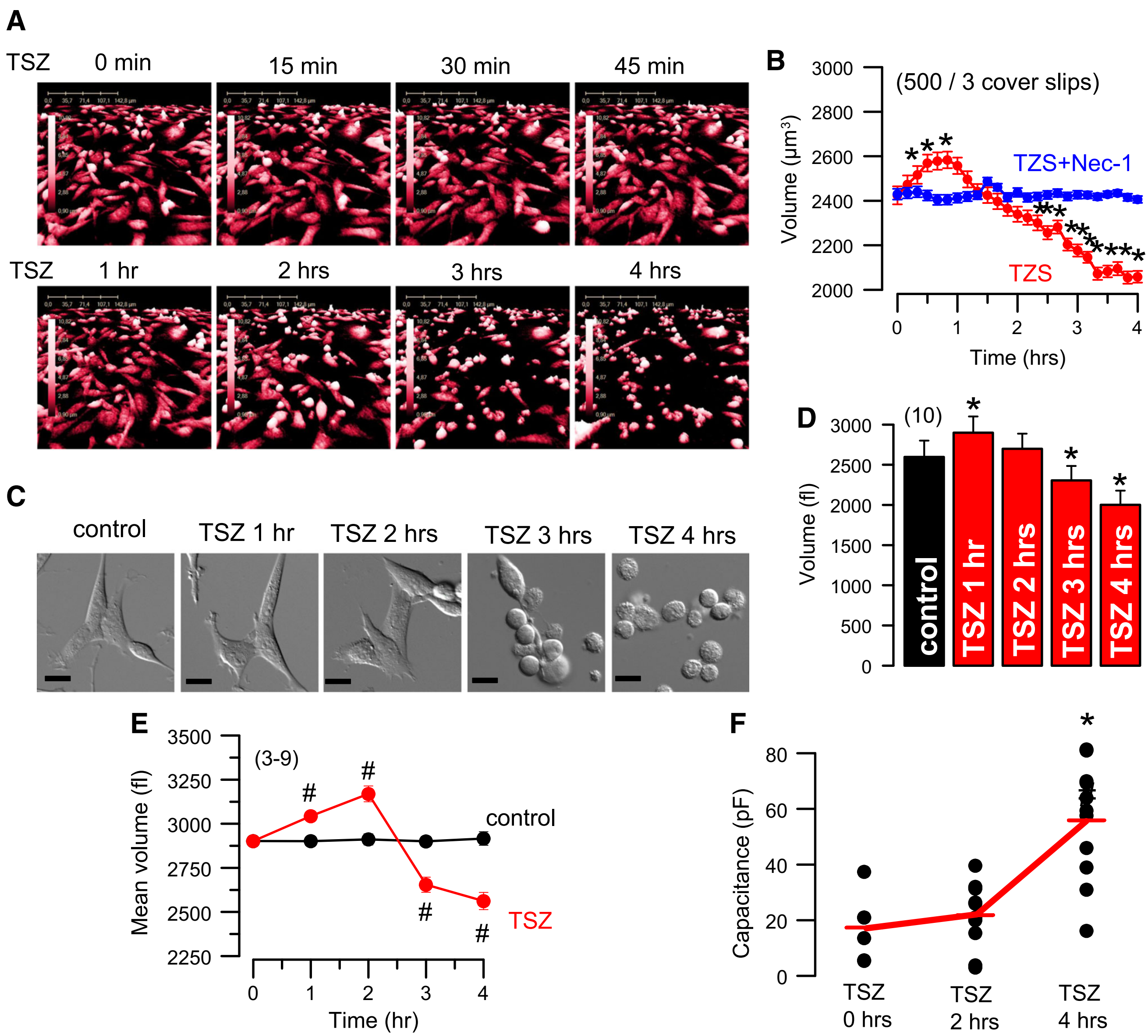

Fig. 2 Morphology of necroptotic cells. **a** 3D-analysis of non-stained NIH3T3 cells using holographic images (HoloMonitor™, I&L Biosystems; Germany). Induction of necroptosis in NIH3T3 cells by necroptotic cocktail TSZ was paralleled by a time-dependent change of cell morphology. TSZ induced rounding up of the cells and increased cell height, leading to an initial cell swelling followed by an overall morphological cell shrinkage. *Vertical scale bar* indicates cell height ranging from 0 to 15.71 µm. **b** Holographic analysis of cell volume confirms initial cell swelling followed by subsequent cell shrinkage. **c** DIC images of NIH 3T3 cells treated with TSZ. **d** Analyzed volumes from individual cells indicating initial cell swelling followed by cell shrinkage. **e** Analysis of TSZ-induced cell volume changes by flow cytometry. Initial cell swelling is followed by cell shrinkage. **f** Measurement of cell membrane capacitance in patch clamp experiments suggesting an increase in cell membrane surface area during necroptosis. *Bar* indicates 10 µm. Mean ± SEM (number of cells). *Significant change in cell volume by TSZ (**b**, $p = 0.00001$–0.0001; **d**, $p = 0.01$–0.03) or capacitance (**f**, $p = 001$) (paired t test). #Significant change in cell volume by TSZ (**e**, $p = 0.0001$–0.001) (ANOVA)

channels (YM58483) were without any impact on intracellular Ca^{2+} changes (Fig. 3c). None of the chemical compounds used here induced cell death on their own when cells were incubated at the given concentrations for up to 24 h. Thus, our data do not confirm large intracellular Ca^{2+} increases during necroptosis, a significant Ca^{2+} influx or a role of TRPM7 channels as reported earlier [16].

To further exclude an essential role of Ca^{2+} influx for necroptotic cell death, we performed the experiments in the complete absence of extracellular free Ca^{2+} using EGTA. Even in the presence of 5 mM EGTA, TSZ-induced necroptosis in NIH3T3 cells was not suppressed (Supplement 4). Moreover, transient oscillatory Ca^{2+} rises observed in necroptotic cells were not abolished in the

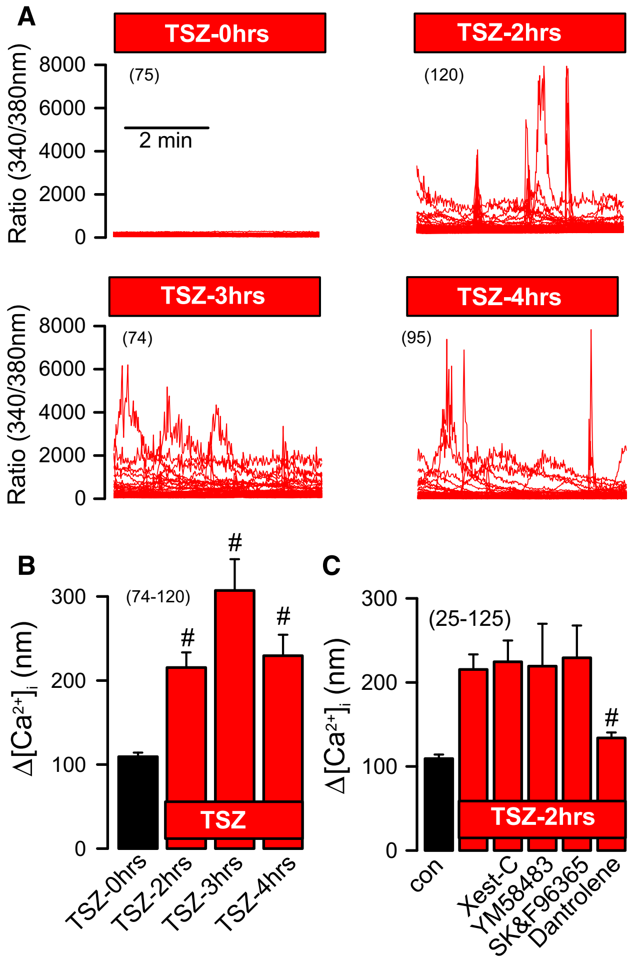

Fig. 3 Ca^{2+} signals in necroptotic cells. Analysis of intracellular Ca^{2+} signals during induction of necroptosis. **a** Ca^{2+} oscillations induced by TSZ. **b** Rise in intracellular Ca^{2+} levels by TSZ. **c** Rise in intracellular Ca^{2+} levels by TSZ was not affected by the (1) inhibitor of IP3 receptors, xestospongin C (1 µM), (2) the inhibitor of ORAI channels, YM58483 (5 µM), or the inhibitor of TRPC channels, SK&F96365 (20 µM), but was *blocked* by dantrolene (10 µM), an inhibitor of ryanodine receptors. *Red bars* indicate the presence of TSZ. Mean ± SEM (number of cells). #Significant increase of intracellular Ca^{2+} levels by TSZ (**b**, $p = 0.0037$, 2 h; $p = 0.001$, 3 h; $p = 0.0015$, 4 h), and inhibition of Ca^{2+} increase by dantrolene (**c**, $p = 0.04$) (ANOVA)

presence of Ca^{2+} free extracellular buffer (data not shown). Additional experiments were performed in TSZ-treated NIH3T3 cells, by chelating intracellular Ca^{2+} using the membrane permeable Ca^{2+} chelator BAPTA-AM. Chelating intracellular Ca^{2+} basically abolished TSZ-induced necroptosis, suggesting an essential role of intracellular Ca^{2+} for necroptosis (Supplement 4). Further experiments were performed in HT_{29} colonic epithelial cells. Removal of extracellular Ca^{2+} did not inhibit, but surprisingly even augmented necroptotic cell death. Moreover, chelating intracellular Ca^{2+} by BAPTA-AM did not inhibit but increased necroptotic cell death (Supplement 5). In addition, in the other cell lines used in the present study, extracellular Ca^{2+} removal had no significant effects on TSZ-induced necroptotic cell death (data not shown). Notably, TSZ induced a comparably small Ca^{2+} increase and activated a tannic acid-sensitive whole cell current in HT_{29} cells (Supplement 6). Taken together, the present data do not confirm the general importance of Ca^{2+} influx for necroptotic cell death.

We further examined whether whole cell currents are activated during necroptotic cell death. Indeed, we observed large outwardly rectifying and time-dependent whole cell currents 4 h after incubation with TSZ (Fig. 4a, b). As replacement of extracellular Cl^- by gluconate ($5Cl^-$) strongly inhibited these currents, the activated currents show features remarkably similar to TMEM16/anoctamin Cl^- channels [18]. Moreover, TSZ-activated currents were inhibited by the ANO6 blocker tannic acid [8, 19] (TA; Fig. 4c). Concentrations of 5–20 µM were used in the present study. These concentrations are not toxic, as they come close to those achieved by consumption of red wine or green tea [20]. Moreover, the activation of the whole cell currents was no longer detected upon siRNA knockdown of ANO6 (Fig. 4d).

To assess a possible contribution of other anoctamins, we analyzed mRNA expression of TMEM16A-K/ANO1-10 in NIH3T3 cells, and found significant levels only for ANO6 and for ANO10, with a minor expression for ANO8 (Fig. 5a, b). ANO6 has been identified as Ca^{2+}-activated phospholipid scramblase and as Ca^{2+}-activated Cl^- channel [9, 21–25]. ANO6 produced outwardly rectifying and time-dependent Cl^- currents and changed cell volume and membrane properties in activated platelets and macrophages [8, 26, 27]. In contrast to ANO6, which is a membrane-localized protein, ANO10 is located predominately in cytosolic compartments and is associated with the ER. Nevertheless, it has been shown to produce membrane currents and to participate in the activation of macrophages [28]. However, siRNA-knockdown of ANO6 and/or ANO10 expression had only a minor inhibitory effect in necroptotic cell death (Fig. 5d). This result is further corroborated by the fact that none of the anoctamin inhibitors were able to attenuate necroptotic cell death (Fig. 5e). An array of inhibitors of Ca^{2+} signaling (such as blockers of Ca^{2+} release or inhibitors of Ca^{2+} influx) showed only minor effects on necroptotic cell death. We, therefore, propose that Ca^{2+} signaling or Ca^{2+}-dependent activation of anoctamins is of minor relevance for necroptosis.

Discussion

The final step during necroptosis requires RIPK3-dependent phosphorylation of MLKL. The formation of putative pMLKL membrane channels has been claimed, which might lead to cell death due to cell swelling and membrane

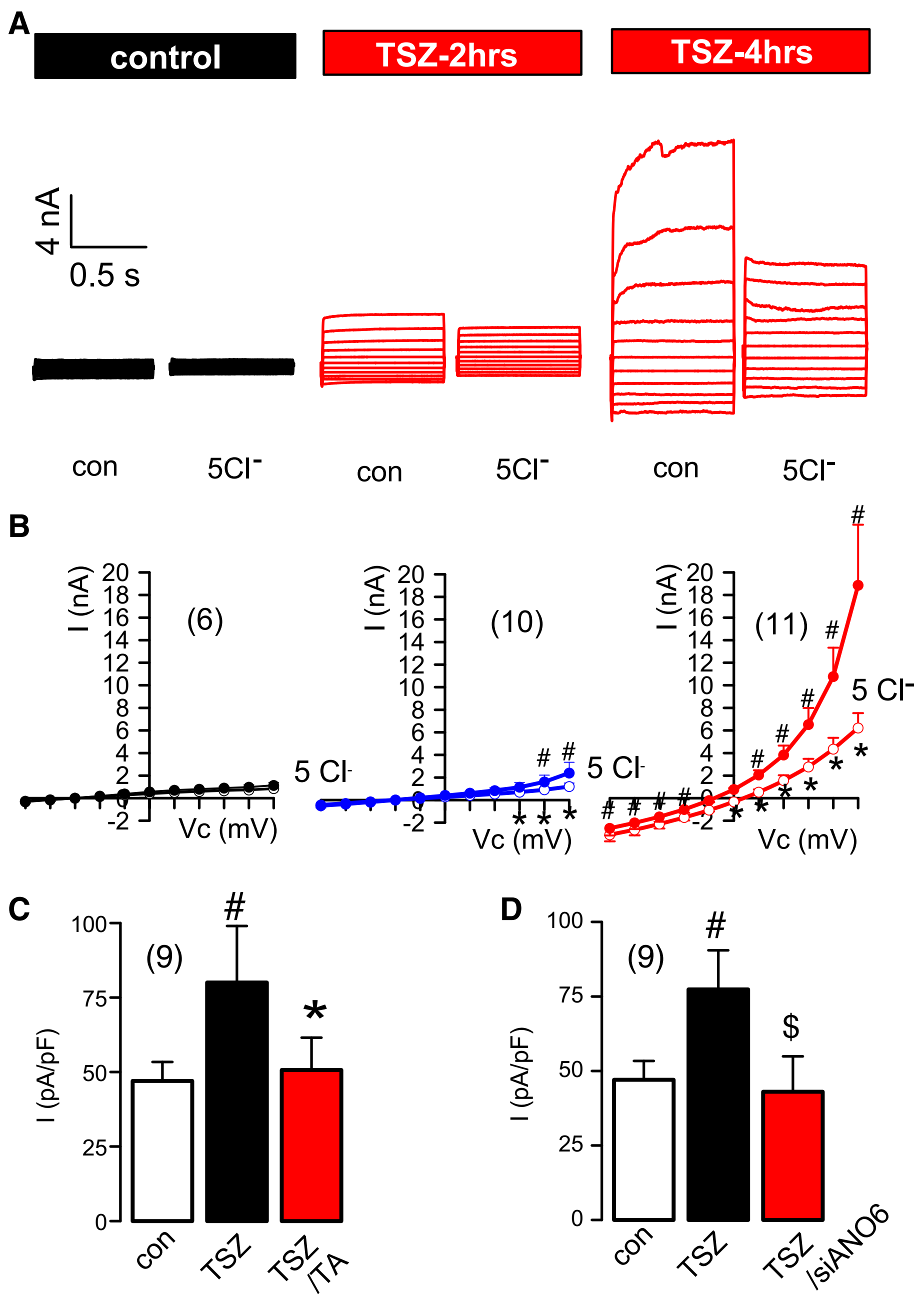

Fig. 4 Whole cell currents in necroptotic cells. **a** Time-dependent whole cell currents activated by TZS, shown at clamp voltages ranging from −100 to +100 mV in steps of 20 mV. **b** Corresponding current voltage relationships indicate the activation of outwardly rectifying whole cell Cl^- currents that are inhibited by replacement of extracellular Cl^- with gluconate ($5Cl^-$). **c** Inhibition of TSZ-activated currents by the ANO6 blocker tannic acid (TA, 5–20 μM). **d** Inhibition of TSZ-activated whole cell currents upon siRNA knockdown of ANO6. Mean ± SEM (number of cells). $^{\#}$Significant increase of whole cell currents by TSZ (**b**–**d**, $p = 0.0015$–0.04) (unpaired t test). *Significant inhibition of whole cell currents by $5Cl^-$ or TA (**b**, $p = 0.001$–0.028; **c**, $p = 0.018$) (paired t test). $^{\$}$Significant inhibition of TSZ-induced whole cell currents by siRNA-ANO6 ($p = 0.039$; unpaired t test)

disintegration [7, 16]. Our present data, however, show little evidence for a nonselective current that would allow permeation of both anions and cations. Moreover, rather than cell swelling, membrane reorganization and cell shrinkage were observed. Finally, evidence for a role of TRPM7 channels during necroptosis of NIH3T3 cells could not be provided in the present study [16]. Our data indicate an only small increase in baseline Ca^{2+} levels, which takes place even in the absence of extracellular Ca^{2+}, indicating a minor role of Ca^{2+} influx for necroptotic cell death. Instead, the data indicate oscillatory Ca^{2+} release from intracellular ER Ca^{2+} stores that is, however, not essential for induction of necroptosis, because the inhibition of Ca^{2+} release by dantrolene does not block necroptotic cell death. [7]. Notably, identical results were obtained in TSZ-treated HT_{29} colonic carcinoma cells, i.e., marginal Ca^{2+} increase with activation of anoctamin currents, which had both little effect on necroptotic cell death (Supplement 6). It is currently unclear whether the Ca^{2+} increase reported here is related to pMLKL-induced mitochondrial permeabilization observed earlier [29]. Notably, in another study, TNF-induced necroptosis was observed even in the absence of mitochondria [11]. Finally, we cannot confirm an essential role of Ca^{2+} influx through Ca^{2+} permeable TRPC

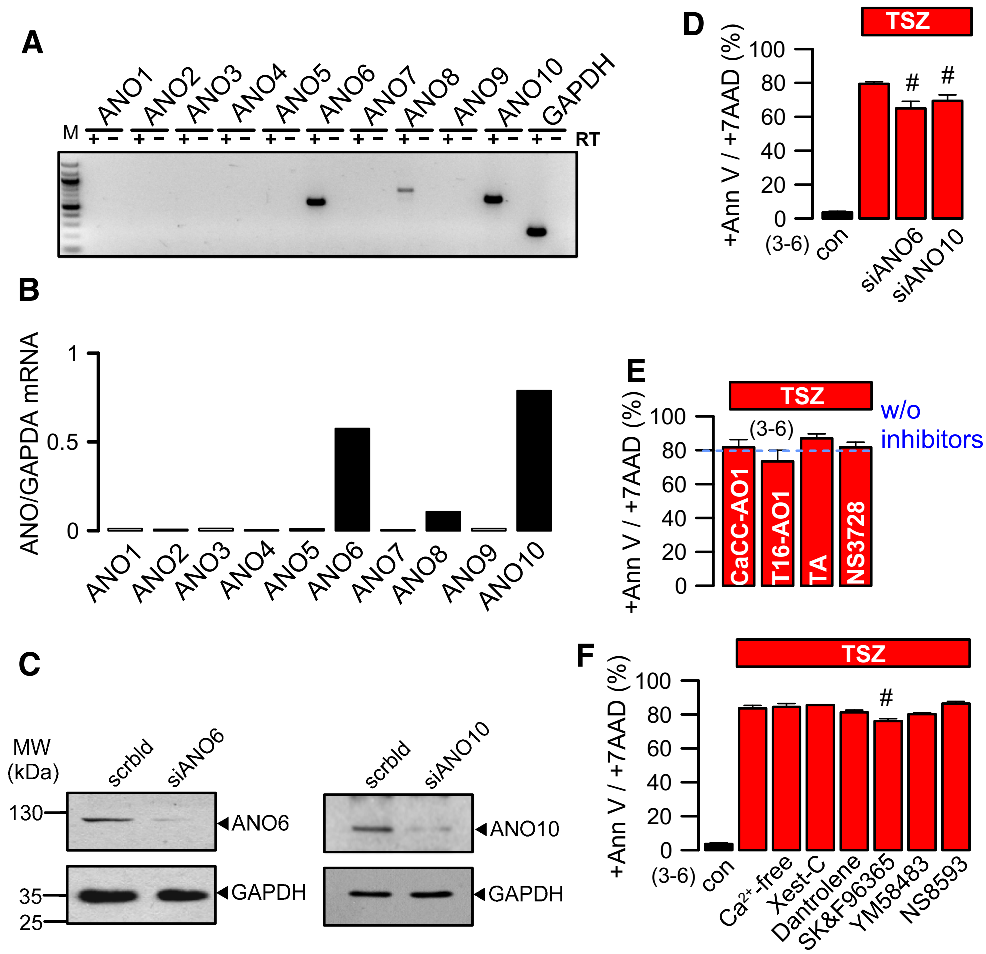

Fig. 5 Minor role of TMEM16F in necroptotic cell death. **a**, **b** RT-PCR analysis of the expression of TMEM16 proteins in NIH3T3 cells indicates dominant expression of TMEM16F (ANO6) and TMEM16K (ANO10). **c** Confirmation of successful protein knockdown by siRNA (72 h). **d** Marginal effects of knockdown of TMEM16F (ANO6) and TMEM16 K (ANO10) on necroptotic cell death. **e** No effects of inhibitors of TMEM16 proteins on necroptotic cell death. $CaCC_{inh}AO1$ (10 µM), $T16_{inh}AO1$ (10 µM), tannic acid (TA, 10 µM), and NS3728 (10 µM). **f** Percentage of necroptotic cells (Annexin V/7-ADD positivity) induced by TSZ and effects of various compounds on cell death. Removal of extracellular Ca^{2+} (Ca^{2+} free), xestospongin C, dantrolene, YM58483, SK&F69365, and the TRPM7-inhibitor NS8593 (10 µM) had no or only marginal effects on cell death. Mean ± SEM (number of cells). #Significant inhibition of necroptosis (**d**, $p = 0.003$–0.021; **f**, $p = 0.017$) (ANOVA)

channels as reported earlier [30]. Thus, neither mitochondrial permeabilization, nor Ca^{2+} release from ER stores seemed to be essential for necroptotic cell death. In addition, our data do not supply evidence for an essential role of TMEM16F/ANO6 or TMEM16K/ANO10 during necroptosis. The recently identified volume-regulated anion channel (VRAC) LRRC8A [4, 5] may also be irrelevant for necroptotic cell death, as neither knockdown of LRRC8A nor the VRAC inhibitor NS3728 interfered with necroptotic cell death (data not shown). Future studies may look into the role of other LRRC8-isoforms, such as LRRC8D [3]. Taken together, the present study demonstrates the activation of anoctamin 6 phospholipid scramblase/ion channel during necroptosis. Activation of ANO6 appears to be a cellular event that takes place parallel to the actual necroptotic cell death, but, nevertheless, may be highly relevant in the physiological/pathophysiological context, e.g., by producing a so-called "eat me" signal [31].

Materials and methods

Cells, cDNA, RT-PCR

Mouse embryonic fibroblasts (NIH3T3) [11], HT_{29} (human colonic carcinoma cells) [32], 16HBE (human immortalized bronchial epithelial cells) [33], H441 (human airway club cells) [34], and L929 (murine skin fibroblasts) cells [35] were grown as described in earlier publications Generation of cDNA for ANO6 and transfection/expression of ANO6 has been report earlier [9]. RT-PCR analyses were performed using the standard conditions and appropriate primers. Cells were treated with 10 ng/ml (NIH3T3; L929) or 100 ng/ml (HT_{29}, 16HBE, H441) TNF-α, 5 μM smac minetic, and 25 μM Z-VAD, (TSZ) to induce necroptosis.

Western blotting

Protein was isolated from cells using a sample buffer containing 50 mM Tris–HCl, 150 mM NaCl, 50 mM Tris, 100 mM dithiothreitol, 1 % Nonidet P-40, 0.5 % sodium deoxycholate, and 1 % protease inhibitor mixture (Sigma, Taufkirchen, Germany). Proteins were separated by 8.5 % SDS-PAGE and transferred to a polyvinyl membrane (GE Healthcare, Munich, Germany). Membranes were incubated with primary anti-ANO1 rabbit polyclonal AB (Davids Biotech, Regensburg, Germany; 1:1000) or anti-phospho-MLKL antibody (Abcam. USA; 1:2000) overnight at 4 °C. Proteins were visualized using horseradish peroxidase-conjugated secondary antibody and ECL detection.

Measurement of [Ca^{2+}]i

Measurement of the intracellular Ca^{2+} concentration was performed as described recently [36]. In brief, cells were loaded either with 5 μM Fura2-AM (to measure global cytosolic Ca^{2+} changes) in Ringer solution at 37 °C for 30 min. Fluorescence was detected at 37 °C, using an inverted microscope IMT-2 (Olympus, Nuremberg, Germany) and a high-speed polychromator system (VisiChrome, Puchheim, Germany). The results were obtained at 340/380 nm fluorescence ratio (after background subtraction). After calibration [36], intracellular Ca^{2+} concentrations were calculated.

Patch clamping

Cells were grown on coated glass cover slips. If not indicated otherwise, patch pipettes were filled with a cytosolic-like solution containing KCl 30, K -gluconate 95, NaH_2PO_4 1.2, Na_2HPO_4 4.8, EGTA 1, Ca -gluconate 0.758, $MgCl_2$ 1.03, D-glucose 5, ATP 3, and pH 7.2. The intracellular (pipette) Ca^{2+} activity was 0.1 μM. Coverslips were mounted in a perfused bath chamber on the stage of an inverted microscope (IM35, Zeiss) and kept at 37 °C. The bath was perfused continuously with Ringer solution at a rate of 8 ml/min. Patch pipettes had an input resistance of 2–4 MΩ when filled with the cytosolic-like (physiological) solution. Currents were corrected for serial resistance. The access conductance was measured continuously and was 60–140 nS. Currents (voltage clamp) and voltages (current clamp) were recorded using a patch clamp amplifier (EPC 7, List Medical Electronics, Darmstadt, Germany), the LIH1600 interface, and the PULSE software (HEKA, Lambrecht, Germany) as well as the Chart software (AD Instruments, Spechbach, Germany). The capacitances were recorded continuously and read directly from the instrument. Data were stored continuously on a computer hard disc and analyzed using the PULSE software. In regular intervals, membrane voltage (*V*c) was clamped in steps of 20 mV from −100 to +100 mV from a holding voltage of −100 mV. Current density was calculated by dividing the whole cell currents by cell capacitance.

Fluorescence-activated cell sorting

Phosphatidylserine exposure to the outer cell membrane of apoptotic cells or at the inner plasma membrane of necrotic cells and incorporation of 7-AAD into necrotic cells was quantified by fluorescence-activated cell-sorting (FACS) analysis. The ApoAlert annexin V–FITC antibody and the 7-AAD antibody were purchased from BD Biosciences.

HoloMonitor

Quantitative phase microscopy was applied to detect cell morphology and to calculate for cell volume [12]. Quantitative phase shift imaging allows for non-invasive long-term imaging of non-labelled cells in cell culture incubators (37 °C, humidified air, 5 % CO_2). Holographic microscopy is used in the HoloMonitor™ time-lapse cytometer (Phase Holographic imaging PHI, Lund, Sweden).

Data and statistics

Data are shown as individual traces or as summaries with mean values ± SEM and number of experiments or cells given in parenthesis. For statistical analysis of unpaired data, ANOVA or unpaired *t* test was used as appropriate. For the statistical analysis of paired data, paired *t* test was used. A *p* value of <0.05 was accepted as statistically significant difference (indicated by $^{\#,\ \$}$ for unpaired data and by * for paired data). Individual *p* values are given in the figure legends.

Acknowledgments This work was supported by DFG SFB699-A7/A12, DFG KU756/12-1, Volkswagenstiftung AZ 87 499, and Medical Faculty of Kiel University (F355910 to SK).

References

1. Kunzelmann K (2016) Ion channels in regulated cell death. Cell Mol Life Sci 73(11–12):2387–2403
2. Lang F, Hoffmann EK (2012) Role of ion transport in control of apoptotic cell death. Compr Physiol 2:2037–2061
3. Planells-Cases R, Lutter D, Guyader C, Gerhards NM, Ullrich F, Elger DA, Kucukosmanoglu A, Xu G, Voss FK, Reincke SM,

Stauber T, Blomen VA, Vis DJ, Wessels LF, Brummelkamp TR, Borst P, Rottenberg S, Jentsch TJ (2015) Subunit composition of VRAC channels determines substrate specificity and cellular resistance to Pt-based anti-cancer drugs. EMBO J 34:2993–3008
4. Voss FK, Ullrich F, Munch J, Lazarow K, Lutter D, Mah N, Andrade-Navarro MA, von Kries JP, Stauber T, Jentsch TJ (2014) Identification of LRRC8 heteromers as an essential component of the volume-regulated anion channel VRAC. Science 344:634–638
5. Qiu Z, Dubin AE, Mathur J, Tu B, Reddy K, Miraglia LJ, Reinhardt J, Orth AP, Patapoutian A (2014) SWELL1, a plasma membrane protein, is an essential component of volume-regulated anion channel. Cell 157:447–458
6. Linkermann A, Green DR (2014) Necroptosis. N Engl J Med 370:455–465
7. Chen X, Li W, Ren J, Huang D, He WT, Song Y, Yang C, Li W, Zheng X, Chen P, Han J (2014) Translocation of mixed lineage kinase domain-like protein to plasma membrane leads to necrotic cell death. Cell Res 24:105–121
8. Ousingsawat J, Wanitchakool P, Kmit A, Romao AM, Jantarajit W, Schreiber S, Kunzelmann K (2015) Anoctamin 6 mediates effects essential for innate immunity downstream of P2X7-receptors in macrophages. Nat Commun 6:6245
9. Tian Y, Schreiber R, Kunzelmann K (2012) Anoctamins are a family of Ca^{2+} activated Cl^- channels. J Cell Sci 125:4991–4998
10. Yu K, Whitlock JM, Lee K, Ortlund EA, Yuan CY, Hartzell HC (2015) Identification of a lipid scrambling domain in ANO6/TMEM16F. Elife. doi:10.7554/eLife.06901
11. Tait SW, Oberst A, Quarato G, Milasta S, Haller M, Wang R, Karvela M, Ichim G, Yatim N, Albert ML, Kidd G, Wakefield R, Frase S, Krautwald S, Linkermann A, Green DR (2013) Widespread mitochondrial depletion via mitophagy does not compromise necroptosis. Cell Rep 5:878–885
12. Depeursinge C, Colomb T, Emery Y, Kuhn J, Charriere F, Rappaz B, Marquet P (2007) Digital holographic microscopy applied to life sciences. Conf Proc IEEE Eng Med Biol Soc 2007:6244–6247
13. Marquet P, Depeursinge C, Magistretti PJ (2013) Exploring neural cell dynamics with digital holographic microscopy. Annu Rev Biomed Eng 15:407–431
14. Molder A, Sebesta M, Gustafsson M, Gisselson L, Wingren AG, Alm K (2008) Non-invasive, label-free cell counting and quantitative analysis of adherent cells using digital holography. J Microsc 232:240–247
15. Okada Y (2006) Cell volume-sensitive chloride channels: phenotypic properties and molecular identity. Contrib Nephrol 152:9–24
16. Cai Z, Jitkaew S, Zhao J, Chiang HC, Choksi S, Liu J, Ward Y, Wu LG, Liu ZG (2014) Plasma membrane translocation of trimerized MLKL protein is required for TNF-induced necroptosis. Nat Cell Biol 16:55–65
17. Wanitchakool P, Ousingsawat J, Sirianant L, MacAulay N, Schreiber R, Kunzelmann K (2016) Cl^- channels in apoptosis. Eur Biophys J. doi:10.1007/s00249-016-1140-3
18. Kunzelmann K, Tian Y, Martins JR, Faria D, Kongsuphol P, Ousingsawat J, Thevenod F, Roussa E, Rock JR, Schreiber R (2011) Anoctamins. Pflugers Arch 462:195–208
19. Namkung W, Thiagarajah JR, Phuan PW, Verkman AS (2010) Inhibition of Ca^{2+} -activated Cl^- channels by gallotannins as a possible molecular basis for health benefits of red wine and green tea. FASEB J 24:4178–4186
20. Ko EA, Jin BJ, Namkung W, Ma T, Thiagarajah JR, Verkman AS (2013) Chloride channel inhibition by a red wine extract and a synthetic small molecule prevents rotaviral secretory diarrhoea in neonatal mice. Gut 63(7):1120–1129
21. Suzuki J, Umeda M, Sims PJ, Nagata S (2010) Calcium-dependent phospholipid scrambling by TMEM16F. Nature 468:834–838
22. Grubb S, Poulsen KA, Juul CA, Kyed T, Klausen TK, Larsen EH, Hoffmann EK (2013) TMEM16F (Anoctamin 6), an anion channel of delayed Ca^{2+} activation. J Gen Physiol 141:585–600
23. Shimizu T, Iehara T, Sato K, Fujii T, Sakai H, Okada Y (2013) TMEM16F is a component of a Ca^{2+} -activated Cl^- channel but not a volume-sensitive outwardly rectifying Cl^- channel. Am J Physiol Cell Physiol 304:C748–C759
24. Sirianant L, Ousingsawat J, Wanitchakool P, Schreiber R, Kunzelmann K (2015) Cellular volume regulation by anoctamin 6:Ca^{2+}, phospholipase A2, osmosensing. Pflügers Arch 468:335–349
25. Kunzelmann K, Nilius B, Owsianik G, Schreiber R, Ousingsawat J, Sirianant L, Wanitchakool P, Bevers EM, Heemskerk JW (2014) Molecular functions of anoctamin 6 (TMEM16F): a chloride channel, cation channel or phospholipid scramblase? Pflügers Arch 466:407–414
26. Mattheij NJ, Braun A, van Kruchten R, Castoldi E, Pircher J, Baaten CC, Wulling M, Kuijpers MJ, Kohler R, Poole AW, Schreiber R, Vortkamp A, Collins PW, Nieswandt B, Kunzelmann K, Cosemans JM, Heemskerk JW (2015) Survival protein anoctamin-6 controls multiple platelet responses including phospholipid scrambling, swelling, and protein cleavage. FASEB J 30:727–737
27. Liu G, Liu G, Chen H, Borst O, Gawaz M, Vortkamp A, Schreiber R, Kunzelmann K, Lang F (2015) Involvement of Ca^{2+} activated Cl^- channel Ano6 in platelet activation and apoptosis. Cell Physiol Biochem 37:1934–1944
28. Hammer C, Wanitchakool P, Sirianant L, Papiol S, Monnheimer M, Faria D, Ousingsawat J, Schramek N, Schmitt C, Margos G, Michel A, Kraiczy P, Pawlita M, Schreiber R, Schulz TF, Fingerle V, Tumani H, Ehrenreich H, Kunzelmann K (2015) A coding variant of ANO10, affecting volume regulation of macrophages, is associated with Borrelia seropositivity. Mol Med 21:26–37
29. Karch J, Kanisicak O, Brody MJ, Sargent MA, Michael DM, Molkentin JD (2015) Necroptosis interfaces with MOMP and the MPTP in mediating cell death. PLoS One 10:e0130520
30. Henriquez M, Armisen R, Stutzin A, Quest AF (2008) Cell death by necrosis, a regulated way to go. Curr Mol Med 8:187–206
31. Segawa K, Nagata S (2015) An apoptotic ‘eat me’ signal: phosphatidylserine exposure. Trends Cell Biol 25:639–650
32. Hayslett JP, Gögelein H, Kunzelmann K, Greger R (1987) Characteristics of apical chloride channels in human colon cells (HT_{29}). Pflügers Arch 410:487–494
33. Kunzelmann K, Koslowsky T, Gruenert DC, Greger R (1994) CAMP-dependent activation of ion conductances in bronchial epithelial cells. Pflügers Arch 428:590–596
34. Faria D, Lentze N, Almaca J, Luz S, Alessio L, Tian Y, Martins JP, Cruz P, Schreiber R, Rezwan M, Farinha CM, Auerbach D, Amaral MD, Kunzelmann K (2012) Regulation of ENaC biogenesis by the stress response protein SERP1. Pflugers Arch 463:819–827
35. Linkermann A, Brasen JH, De Zen F, Weinlich R, Schwendener RA, Green DR, Kunzendorf U, Krautwald S (2012) Dichotomy between RIP1- and RIP3-mediated necroptosis in tumor necrosis factor-alpha-induced shock. Mol Med 18:577–586 **(Cambridge, Mass)**
36. Schreiber R, Uliyakina I, Kongsuphol P, Warth R, Mirza M, Martins JR, Kunzelmann K (2010) Expression and Function of Epithelial Anoctamins. J Biol Chem 285:7838–7845